On the imaging of biogenic and anthropogenic surface films on the sea by radar sensors

Martin Gade

Institute of Oceanography, University of Hamburg, Hamburg, Germany

Abstract. Radar signatures of sea surface films of different origin are investigated, which have been acquired by airborne and spaceborne multi-frequency/multi-polarisation microwave sensors during the *Spaceborne Imaging Radar-C/X-Band Synthetic Aperture Radar* (SIR-C/X-SAR), missions in 1994, as well as by the ERS SAR in 1996-98. During SIR-C/X-SAR, controlled surface film experiments were performed in the German Bight by deploying various quasi-biogenic substances and mineral oil on the sea surface, in order to study the radar signatures caused by surface films of different visco-elastic properties. In general, our results show that multi-frequency capabilities, rather than multi-polarisation capabilities, are needed for a radar-based system for the discrimination of marine surface films. We show that, under high wind conditions (> 10 m s^{-1}), a discrimination between the different kinds of surface films is very difficult, whereas at low to moderate wind speeds (≤ 5 m s^{-1}) a discrimination seems to be possible. This finding is supported analytically by means of a new model for the wave number-dependent radar contrast at high wind speeds (> 10 m s^{-1}) and statistically through the analyses of more than 700 ERS SAR images. In addition, results of laboratory experiments are presented that were carried out in the wind-wave tank of the University of Hamburg. At certain wind-speed ranges a different damping of bound and freely propagating surface waves by monomolecular surface films is observed, which may explain the high radar contrasts measured by the microwave sensors.

1 Introduction

The damping of short gravity-capillary ocean surface waves by biogenic and anthropogenic surface films is a well known phenomenon and has been subject of various investigations (Gade et al. 1998a, and literature cited therein). At oblique incidence angles short ocean surface waves are responsible for the backscattering of microwaves of comparable wave-

lengths (Bragg scattering, see Valenzuela 1978), thus, wave damping by oceanic surface films causes a reduction of the measured radar backscatter. For this reason, dark patches visible on synthetic aperture radar (SAR) images of the ocean surface can often be related to oil spills or natural slicks floating on the sea surface.

The layer thickness of a mineral oil spill is much larger than that of a monomolecular sea slick, which results in different visco-elastic properties and, therefore, in a different damping of the ocean surface waves (Alpers and Hühnerfuss 1988). Results of laboratory experiments showed that Marangoni damping is the dominant mechanism for the damping of short sinusoidal gravity waves by monomolecular slicks (Hühnerfuss 1986). Following Marangoni damping theory, monomolecular surface films exhibit a resonance-like damping behaviour (at wave numbers of about 100 $radm^{-1}$), whereas this distinct damping maximum is missing for (thick) mineral oil spills.

Since the application of a single-frequency, fixed incidence radar system (like the C-band SAR aboard the ERS satellites) can provide information on the damping of ocean surface waves at only one single Bragg wavelength, multi-frequency radar techniques have already been used to obtain more extended information on the damping behaviour of the detected surface films (e.g., Gade et al. 1998c). However, during recent field experiments with artificial monomolecular surface films, a distinct damping-maximum at intermediate wave numbers was not measured (Gade et al. 1998c). Thus, additional terms describing the energy fluxes on the water surface, like the energy input by the wind, wave breaking, and non-linear wave-wave interaction, have to be taken into account for the development of theoretical models that can explain the measured damping of small ocean surface waves by different surface films.

During the two Shuttle Imaging Radar C-/X-Band Synthetic Aperture Radar (SIR-C/X-SAR) missions in April and October, 1994, surface films of different visco-elastic properties were deployed in the German Bight of the North Sea, in order to simulate different biogenic and anthropogenic ocean surface films. The aim of these experiments was to investigate whether active microwave techniques are capable of yielding information, on the one hand, on the damping behaviour of different surface films and, on the other hand, on the damping behaviour of one substance under different environmental conditions. Here we briefly present the results of these experiments obtained by a 5-frequency/multi-polarisation scatterometer, and by the 3-frequency/multi-polarisation SIR-C/X-SAR. They are complemented by statistical analyses of more than 700 ERS SAR images acquired over different parts of European coastal waters and by results of laboratory studies performed in a wind-wave tank. For a more de-

tailed description of these results the reader is referred to Gade (1996) and to the papers by Gade et al. (1998a,b,c).

2 Results obtained from measurements with HELISCAT

During the two SIR-C/X-SAR missions in April and October, 1994, radar backscatter measurements were carried out with a 5-frequency/multi-polarisation scatterometer flown on a helicopter. This scatterometer, called HELISCAT, works at 1.25, 2.4, 5.3, 10.0, and 15.0 GHz (L-, S-, C-, X-, and Ku-band, respectively) and is capable of performing radar backscatter measurements at different incidence angles.

During all measurements, monomolecular slicks consisting of oleyl alcohol (OLA) were deployed, thus allowing for an investigation of the dependence of the damping behaviour on different environmental conditions, in particular, on wind speed. Even though it is known to simulate biogenic slicks not optimally, this substance was already deployed during several earlier campaigns, because its strong damping capabilities make it easy to be detected by microwave sensors. In addition to OLA, slicks consisting of oleic acid methyl ester (OLME) and triolein (TOLG) were deployed, which both represent compounds of natural surface films. Because of their molecular structure, these substances form monomolecular surface films (i.e., slicks with a thickness of only one molecule). Depending on wind and wave conditions, however, these slicks may be locally disrupted, thus causing a large scatter in the measured radar contrast (Figures 1 and 2). The measurements were performed shortly after the slick deployment, when the slicks were fully spread, in order to avoid any data spoiling by slick aging effects. The measured damping ratios (i.e., the ratios of the relative backscattered radar power from a slick-free and a slick-covered water surface) are shown in Figure 1.

It can be concluded that, under all wind speed conditions, the measured damping ratios increase with increasing Bragg wave number and that the maximum damping decreases with increasing wind speed. These two findings cannot be explained by pure Marangoni damping theory which describes the damping of small sinusoidal water surface waves by monomolecular slicks and which predicts a distinct damping maximum at intermediate wave numbers of approx. 100 rad m^{-1} (Hühnerfuss 1986). In addition, wind-induced effects, primarily the energy input into the wave spectrum, have to be considered, as well.

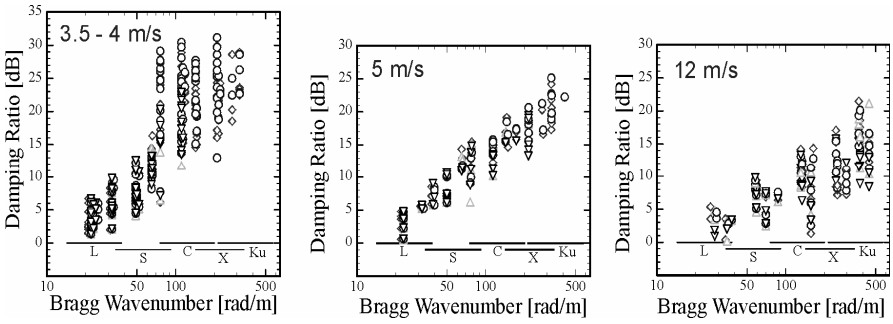

Fig. 1. Damping ratios measured by HELISCAT over an oleyl alcohol (OLA) slick at different wind speeds (**left:** 3.5–4 m s^{-1}; **middle**: 5 m s^{-1}, **right:** 12 m s^{-1}). Diamonds, circles, and grey triangles denote HH, VV, and VH/HV polarisation, respectively

In order to explain their experimental results obtained at high wind speeds (12 m s^{-1}, where the energy input by the wind is larger than the viscous dissipation in the whole Bragg wave number range) quantitatively Gade et al. (1998c) developed an analytical model for the damping ratios that is based on the assumption that the spectral action is balanced (Hasselmann 1960), i.e.

$$\frac{\sigma^{(0)}(k)}{\sigma^{(s)}(k)} = \frac{\Psi_0(k)}{\Psi_s(k)} = \frac{N_0(k)}{N_s(k)} = \frac{S_{wi}^{(s)} - S_{vd}^{(s)}}{S_{wi}^{(0)} - S_{vd}^{(0)}} \cdot \frac{S_{br}^{(0)} - S_{nl}^{(0)}}{S_{br}^{(s)} - S_{nl}^{(s)}} \tag{1}$$

where σ is the radar backscattering at a (Bragg) wave number k, $\Psi(k)$ is the wave spectrum, $N(k)$ is the wave action, and S_{wi}, S_{vd}, S_{br}, and S_{nl} are the source terms for the wind input, viscous dissipation, wave breaking, and nonlinear interaction, respectively. The indices "0" and "s" denote a slick-free and a slick-covered water surface. Gade et al. (1998c) included analytical expressions for the wind input (Phillips 1985) and the wave breaking (Donelan and Pierson 1987) and assumed that the nonlinear interaction is much smaller than the energy flux caused by wave breaking (which should be the case under high wind conditions). They found the following expression for the measured damping ratios:

$$\frac{\sigma^{(0)}(k)}{\sigma^{(s)}(k)} \approx \frac{\beta_s - 2\Delta_s c_g}{\beta_0 - 2\Delta_0 c_g} \cdot m^{\Delta n - 4} \left(2u_* \cdot \sqrt{\frac{|\cos\varphi| k}{g}} \right)^{\Delta n} \tag{2}$$

where β is the coefficient for the wind energy input given by Plant (1982), Δ is the coefficient for viscous dissipation, c_g is the group velocity of the water waves, u_* is the wind friction velocity, φ is the azimuth angle be-

tween wind and wave propagation direction, and g is the acceleration of gravity. The parameters m and Δn describe the reduction of u_* and of the wave breaking, respectively, in the presence of a slick (for more details see Gade et al. (1998c)):

$$m = u_*^{(s)} / u_*^{(0)}$$
$$\Delta n = n_0 - n_s \tag{3}$$

where n_i are the exponents in the analytical description of the wave breaking source term, $S_{br} \sim (k^4 \Psi)^n$. Following the results of earlier field measurements performed by Stolte (pers. commun.), m was set to 0.7 and 0.9 for the strong (leeward) and weak (windward) damping parts of the surface films, respectively. Considering the different impact of the weak and strong damping parts of a surface film on wave breaking the parameter Δn is ranging from 0.7 (weak damping substance oleic acid methyl ester) to 3.5 (strong damping substance oleyl alcohol).

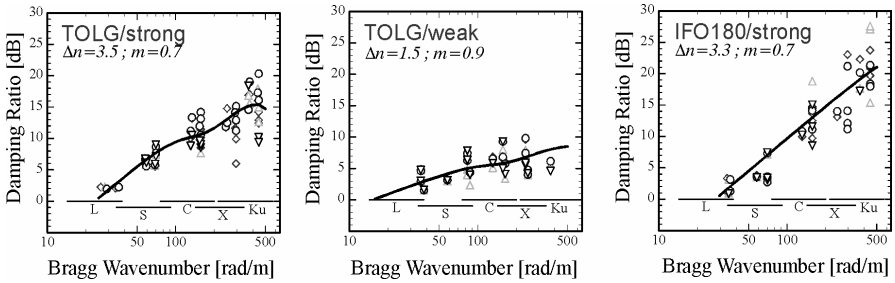

Fig. 2. Same as Figure 1, but for the strong (**left**) and weak (**middle**) damping parts of a triolein (TOLG) slick and the strong damping parts of a mineral oil (IFO180, **right**) spill under high wind conditions (12 m s^{-1}). The solid lines added into each diagram denote model results (see (1)) using the respective parameters m and Δn given in the panels. Diamonds, circles, and grey triangles denote HH, VV, and VH/HV polarisation, respectively

Note that in this parameterisation m and Δn describe the reduction, but not the absolute value, of the source terms for wind input and wave breaking, respectively.

Deploying their model Gade et al. (1998c) were able to explain the continuous increase in the measured damping ratios with Bragg wave number. A comparison of some experimental and model results is shown in Figure 2.

It is obvious that this model can well reproduce the measured damping ratios and, moreover, that the absence of the expected Marangoni damping maximum at intermediate Bragg wave numbers (approx. 100 rad m^{-1}) can

be interpreted. Furthermore, the model can explain the similarities between the results obtained from quasi-biogenic (TOLG) and anthropogenic (IFO180) surface films under high wind conditions.

3 Results obtained from analyses of SIR-C/X-SAR data

Various SIR-C/X-SAR images showing biogenic and anthropogenic surface films at different parts of the world's oceans were analysed, in order to investigate whether or not SIR-C/X-SAR is capable of discriminating between biogenic and anthropogenic oceanic surface films. Using SAR images of the surface film experiments in the German Bight of the North Sea, again, we found that the measured damping ratios strongly depend on the wind speed, which is in accordance with the results obtained by HELISCAT (see Figure 1). The results obtained from SAR images of various biogenic and anthropogenic surface films are shown in Figures 3 and 4, respectively. The classification between biogenic and anthropogenic surface films was made based on the shape and the size of the observed surface films. E.g., the SAR images shown in Figure 3 show typical signatures of biogenic surface films encountered in large sea areas during ongoing algal blooms: the surface-active material accumulates on the water surface and the long, narrow, dark streaks follow the surface currents. In contrary, signatures caused by spilled mineral oil look different: the dark elongated patch in Figure 4 is very likely caused by an oil spill, because of its irregular shape and the fact, that its contrast is independent of the different wind speed on either sides of the varying wind speed in that very area. In general, however, no sampling of any film material was done for our studies.

It is obvious that biogenic surface slicks cause a strong damping at L-band (Figure 3), whereas anthropogenic oil spills cause low L-band damping ratios (Figure 4). Considering the large scatter of the data, the observed damping ratios at C- and X-band are similar, which, particularly at C-band, is due to an insufficient signal-to-noise ratio of the SIR-C/X-SAR system.

The presented results, however, show that multi-frequency SAR imagery yields more information about the damping characteristics of oceanic surface films than single-frequency SAR imagery. This is, in turn, needed for a better discrimination between different kinds of surface films, particularly under low to moderate wind conditions. Moreover, our results show that L-band data is crucial for a successful discrimination of different surface films. Although OLA represents natural slicks, its damping ratios look similar to those of mineral oil spills. A possible reason for this is the limited spatial extent of these films. In contrast, natural slicks usually

cover large areas of the sea surface, thus being more effective in damping even longer (metre) waves.

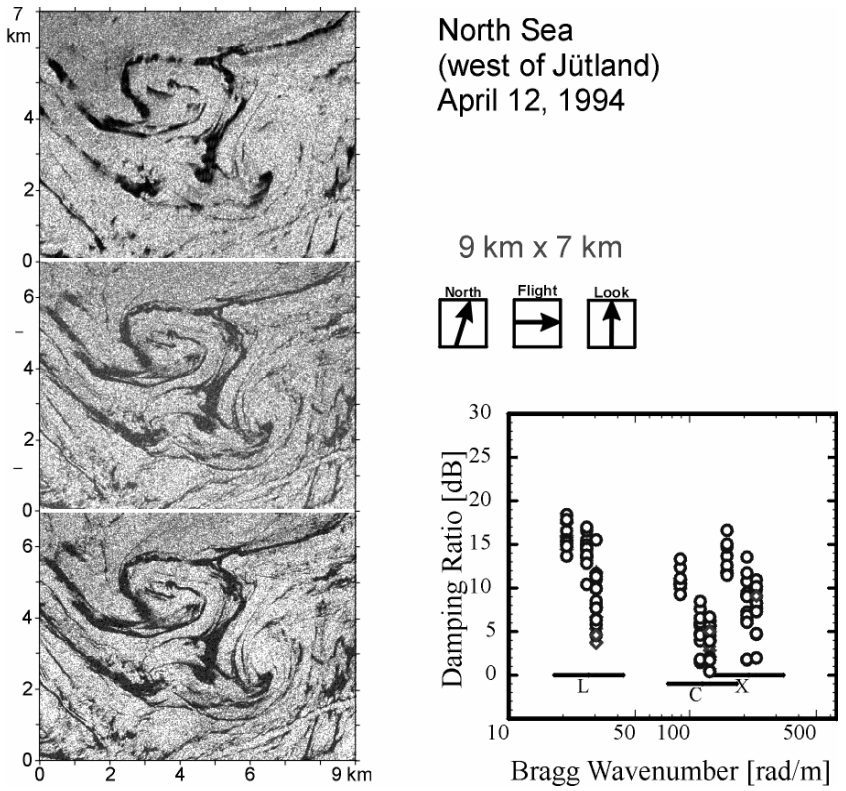

Fig. 3. Left side: SIR-C/X-SAR images of the same spot of the North Sea acquired during the first shuttle mission on April 12th, 1994, and showing signatures of natural surface films (image dimensions 7 by 9 km). The images were acquired at L-, C-, and X-band (from **top to bottom**), VV-polarisation. On the **bottom right**, damping ratios obtained from SIR-C/X-SAR images of various natural slicks at low to moderate wind speeds (< 7 m s^{-1}) are shown. Diamonds and circles denote HH and VV polarisation, respectively

In summary, multi-frequency SAR imagery is advantageous to the recognition and classification of oceanic surface films; that is, important additional information can be inferred from these SAR data. The evidence shows that under low to moderate wind conditions, multi-frequency radar techniques are capable of discriminating between the different kinds of surface films, whereas at high wind conditions a discrimination (on a basis of damping measurements) is impossible (for examples for high wind speed see the paper by Gade et al. (1998b)).

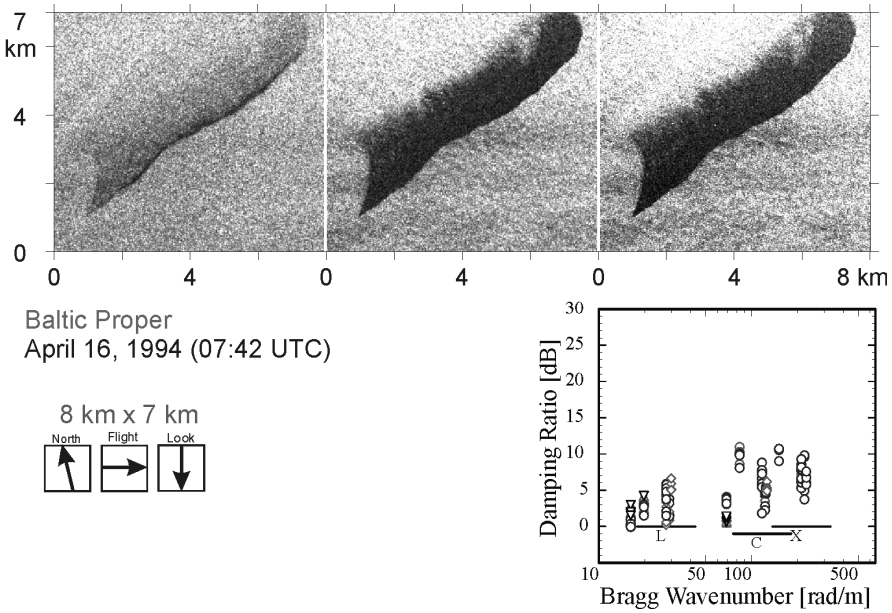

Fig. 4. Upper row: SIR-C/X-SAR images of the same spot of the Baltic Proper acquired during the first shuttle mission on April 16th, 1994, and showing signatures of a mineral oil spill (image dimensions 8 by 7 km). The images were acquired at L-, C-, and X-band (from left to right), VV-polarisation. On the **bottom right**, damping ratios obtained from SIR-C/X-SAR images of various mineral oil spills at low to moderate wind speeds (< 7 m s^{-1}) are shown. Diamonds, circles, and triangles denote HH, VV, and HV/VH polarisation, respectively

4 Statistical Analysis of ERS SAR Data

Gade et al. (2000) analysed more than 700 ERS SAR images of European marginal waters (acquired between December 1996 and November 1998 over the Baltic Sea, the North Sea, and the northwestern Mediterranean Sea) with respect to the detectability of marine oil pollution. Model wind speeds provided by the Deutscher Wetterdienst (DWD, German Weather Service) were used to get an estimate of the influence of the mean local meteorological conditions (namely of the wind speed) on the overall detectability of marine oil pollution. The model results for the three test areas, each for the entire period of SAR image acquisition (December 1996 until November 1998), are shown in Figure 5. The upper row contains the values calculated for the summer periods (April – September) and the

lower row contains the values calculated for the winter periods (October – March). The maximum mean wind speed in the Baltic Sea test area (left column of Figure 5) lies between 8 and 9 m s^{-1} during summer and between 9 and 10 m s^{-1} during winter. The corresponding values for the North Sea test area (middle column) are 7 and 8 m s^{-1} (summer) and 10 and 11 m s^{-1} (winter), and for the northwestern Mediterranean Sea test area they are 6 and 7 m s^{-1} (summer) and 8 and 9 m s^{-1} (winter), respectively. Thus, on average, oil spill detection using SAR techniques should be most successful in the northwestern Mediterranean Sea during the summer period, and it should be least successful in the North Sea test area during winter period.

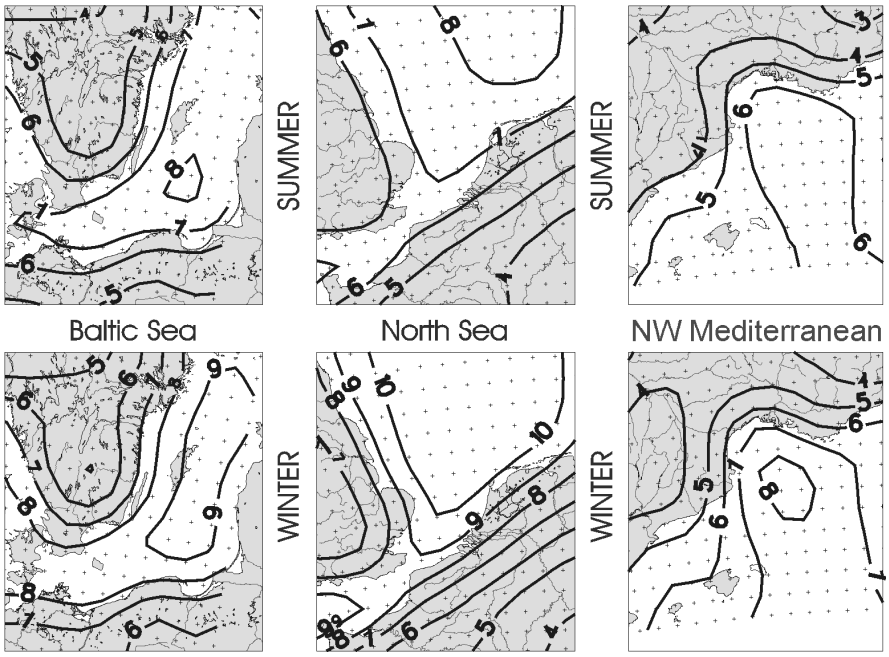

Fig. 5. Mean wind speeds for the three test areas, as derived from a numerical model driven by the DWD. In the upper row the mean wind speeds are shown for summer periods (April – September) and in the lower row for winter periods (October – March)

Gade and Redondo (1999) used the same data set to derive areas of mean oil pollution by taking into account those dark patches in the SAR images that show a significant reduction of the radar backscatter. In all three regions they found more oil pollution during summer months (April – September) than during winter months (October – March), which they

explained by the overall higher wind speeds in all test areas during winter time. Moreover, the northwestern Mediterranean Sea seemed to be the test area with highest detected oil pollution, whereas the pollution seemed to be lowest in the Baltic Sea. They concluded that this might be caused by the difference in mean wind speed, which in turn causes a different visibility of oil pollution in SAR images. (However, it is of course also possible that the northwestern Mediterranean Sea is simply the most polluted test area.)

For our improved statistical analysis we included the mean local windspeed, as derived from interpolated values of the DWD model. As a first step we calculated the distribution of the detected oil spills with wind speed. As shown in the upper left panel of Figure 6 most oil spills were detected at mean (modelled) wind speeds between 3 m s^{-1} and 4 m s^{-1}. The upper right panel of Figure 6 shows the wind speed distribution of the DWD model with a maximum between 5 m s^{-1} and 6 m s^{-1}. The lower panel of Figure 6 shows the "normalised oil spill visibility" (NOSV) calculated as the (normalised) ratio of the two above.

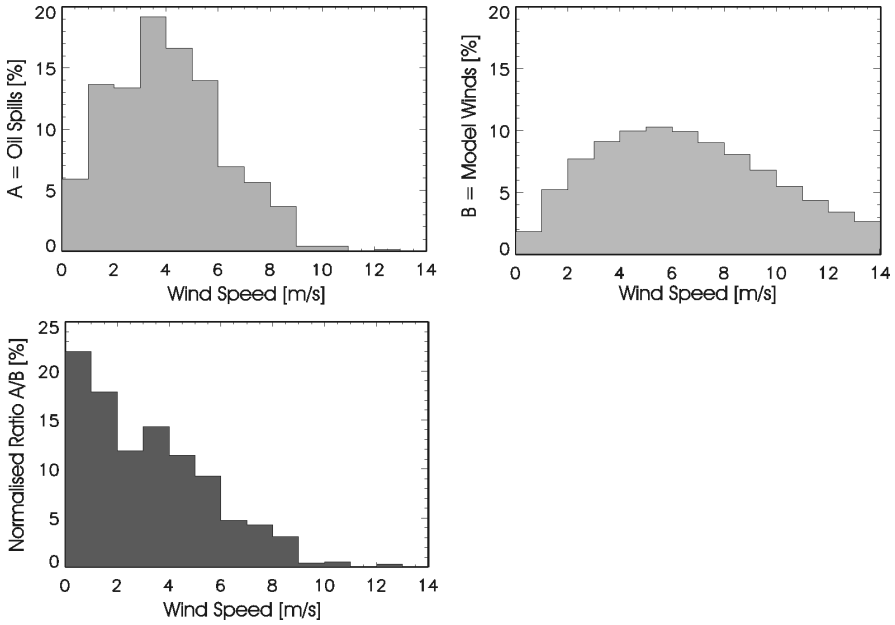

Fig. 6. upper left: histogram of the distribution of detected oil pollution as function of wind speed; **upper right:** distribution of the DWD model winds; **lower left:** "normalised oil spill visibility" calculated as the ratio of the histograms for oil spills and model winds

The NOSV gives a better estimate of the detectability of marine oil pollution, independently of the local wind conditions of this particular study. These results show that higher wind speeds cause lower detectability of oil pollution, and the maximum (model) wind speed where oil spill detection in European coastal waters can be inferred. In particular, at wind speeds below 7 m s^{-1} oil spills are well detectable, whereas above 10 m s^{-1} wind speed the definite detection of marine oil pollution seems to be almost impossible. At wind speeds between 7 and 10 m s^{-1} the detectability of oil spills is rather low. These results can explain why less oil pollution was detected in the northern test areas during winter time. E.g., the mean wind speed in the central North Sea during winter time lies above 10 m s^{-1} (Figure 5), thus making it unlikely that every oil spill in that area was detectable by SAR sensors.

5 Results obtained from laboratory measurements

In order to complement the results of the radar backscatter measurements on the open sea, laboratory measurements of the wave amplitude and slope and of the radar backscatter at X- and Ka-band were carried out in a wind-wave tank with mechanically generated gravity waves as well as with wind-generated waves on a slick-free and a slick-covered water surface. In this paper, we concentrate on the results of the radar measurements with wind-generated waves. For a full description of the obtained results the reader is referred to Gade et al. (1998c).

The measurements were carried out in the wind-wave tank of the University of Hamburg, which is 26 m long and 1 m wide. The mean water depth is 0.5 m, the wind tunnel height is 1 m, and the effective fetch is 19.5 m. The measurement area was at a fetch of 15.5 m. The scatterometers used for the present investigation are working at 9.8 GHz (X-band) and 37 GHz (Ka-band) and the measurements were carried out with upwind looking radar antennae and at VV-polarisation.

Figure 7 shows the measured radar Doppler shifts, both at X- and Ka-band, for the entire wind speed range. The solid and dashed lines in both panels denote theoretical Doppler shifts assuming freely propagating Bragg waves and Bragg waves bound to the dominant wind waves, respectively. We can conclude that the X-band backscattering from a slick-free water surface at low wind speeds (up to approximately 4.5 m s^{-1}) and long fetches (15.5 m in our investigation) is determined mainly by bound waves, whereas the Ka-band backscatter is caused by both bound and freely propagating Bragg waves. For wind speeds higher than 4.5 m s^{-1} the X-band backscattering in our experiments is caused by both parasitic har-

monics and freely propagating Bragg waves, whereas the Ka-band backscatter is caused mainly by freely propagating Bragg waves. In particular, the generation of freely propagating wind waves results in a reduction of the X-band Doppler shift at wind speeds of 4.5-5 m s^{-1}, which is less distinct at Ka-band.

When comparing the results obtained by different authors, one has to take into account the different experimental set-ups, which may lead to different results. In particular, the existence of bound (Bragg) waves does not only depend on the wind speed and frequency of the gravity waves but also, for example, on the fetch length and the wave age (which may strongly differ in different experimental set-ups). Therefore, we suspect that on the open ocean X- and Ka-band Bragg waves are encountered that are both freely propagating and bound to gravity waves (which in turn may be modulated by the long ocean waves).

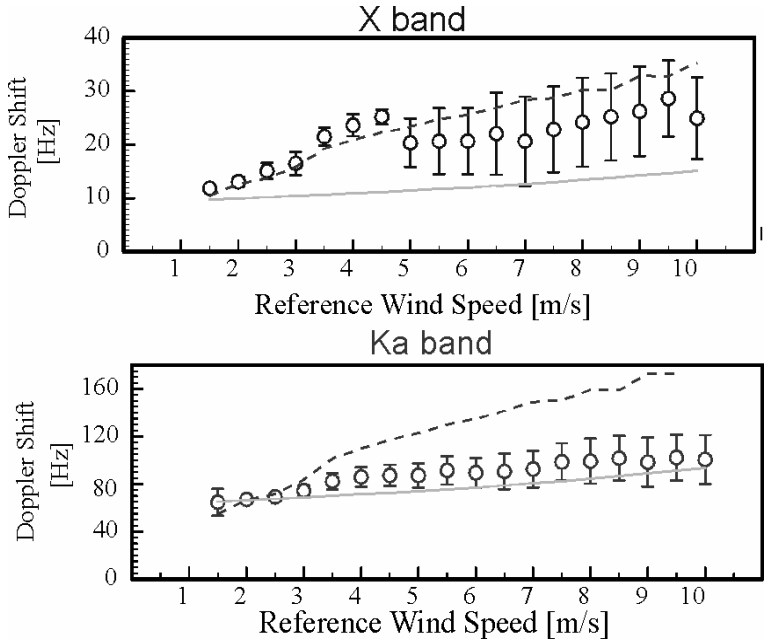

Fig. 7. Measured X- and Ka-band Doppler shifts as function of the reference wind speed. The measurements were performed with a slick-free water surface. Additionally inserted into each diagram are the theoretical curves assuming bound (dashed line) and freely propagating (solid line) Bragg waves

The X- and Ka-band Doppler shifts measured from wind-generated waves on a water surface covered with oleyl alcohol (OLA) are shown in Figure 8. It is obvious that the coverage of the water surface with a sur-

face-active substance has a strong influence on the generation of bound waves at the crests of the gravity waves. At intermediate wind speeds of approximately 6 m s^{-1} the X-band backscatter is mainly caused by bound Bragg waves, and the Ka-band backscatter is caused by both bound and freely propagating Bragg waves. In the wind speed range between 7 and 9 m s^{-1}, where the short gravity waves are strongly damped by the OLA slick, both the X- and Ka-band backscatter are caused only by freely propagating waves. This wave damping behaviour of the OLA slick can explain the strong damping of the radar backscatter in this particular wind speed range as well as the fact that the measured wave damping exceeds the values predicted by Marangoni damping theory for this (water wave) frequency range.

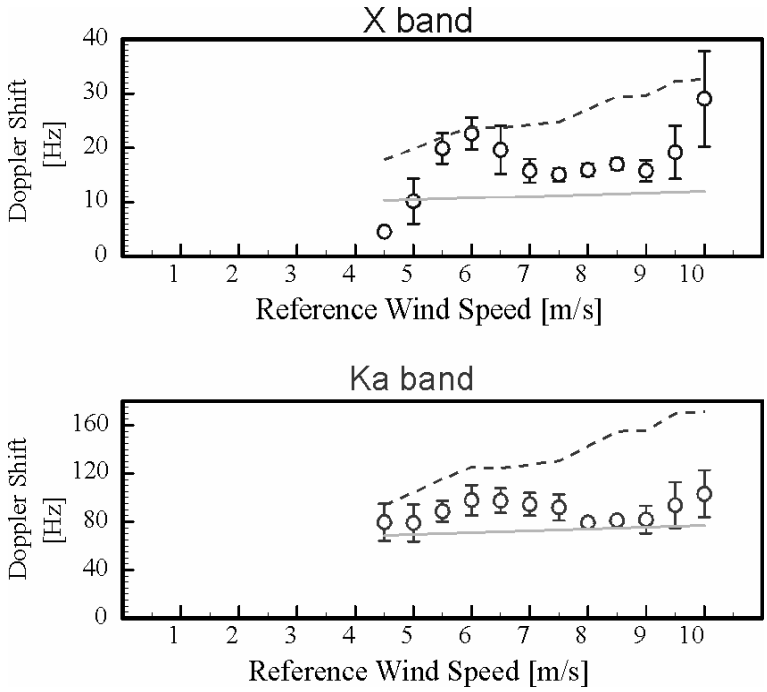

Fig. 8. Same as Figure 7, but for a water surface covered with oleyl alcohol (OLA). The minimum wind speed for the excitation of ripple waves on a slick-covered water surface is about 4.5 m s^{-1}

These results obtained from a slick-covered water surface are of great importance for the interpretation of measured reductions of the radar backscattering by oceanic surface films (see the preceding sections). However, we also note that results obtained from wind-wave tank experiments can-

not be readily transferred to the open ocean. Moreover, the described effects are obviously strongly dependent on the experimental conditions (i.e., on the fetch and the tank dimensions), so that only field experiments (e.g., similar measurements of the radar backscattering performed on the open ocean) can prove our assumption that bound Bragg waves have an important impact on the measured radar signal from the ocean surface. At least, taking our results into account, we can expect reductions of the radar backscatter at X-, Ku-, and Ka-band that are higher than those predicted by Marangoni damping theory. This has indeed been observed.

6 Summary and Conclusions

The results obtained by HELISCAT showed that the damping behaviour (i.e., the ratio of the radar backscatter from a slick-free and a slick-covered water surface) of the same substance strongly depends on the wind speed, which can be explained by means of the source terms of the action balance equation. Thus, we developed a model to simulate measured damping ratios for different surface films at high wind speeds (> 10 m s^{-1}, where the energy input by the wind is larger than the viscous dissipation). The simulated values are in good agreement with the experimental results.

We have analysed SIR-C/X-SAR images from natural surface films and mineral oil spills and have compared the measured damping ratios. It turns out that the radar signatures are most different at L-band (where the signal-to-noise-ratio is sufficiently high). For mineral oil spills the damping ratio increases with Bragg wave number, whereas for natural surface films a minimum of the damping behaviour is measured at C-band (even when the signal-to-noise ratio very often is insufficient).

No significant dependence of the radar contrast on the polarisation was found, whereas it strongly depends on radar frequency. Thus, multi-frequency capabilities are recommended for any radar-based system for the discrimination of oceanic surface films, but not multi-polarisation capabilities. Furthermore, we conclude that the discrimination of natural and man-made surface films seems to be possible at low to moderate wind speeds whereas it is impossible at high wind speeds (see the results obtained at 12 m s^{-1} wind speed, Figures 1 and 2).

It is remarkable that, over each surface film deployed during our field experiments, SIR-C/X-SAR measured lower damping ratios than HELISCAT (Figure 9). These differences are independent of the deployed substance and of wind speed, but not of Bragg wave number. Possible explanations for this finding may include different resolution scales (25 m for the SAR system, the footprint dimensions of the HELISCAT systems are

between a few meters and about 100 m, depending on incidence angle and radar band), while time differences and state of evolution of the slick in our opinion play a minor role. Additional systematic investigations are required in order to answer these questions.

The analysis of a large number of ERS SAR data revealed improved statistical information on the oil pollution of European marginal waters. The results show that the consideration of local environmental conditions (namely the local wind speed) improves the statistical results significantly: the Baltic Sea seems to be only slightly less polluted than the northwestern Mediterranean, which is not in accordance with results from earlier studies where local wind speeds had not been taken into account.

The results from the wind-wave tank measurements show that at X- and Ka-band the radar backscattering from a slick-free water surface is caused by bound as well as by free propagating ripples. In the presence of a monomolecular surface film at certain wind speeds only bound or only free propagating ripples are responsible for the backscattering at X-band, which can explain higher measured damping ratios.

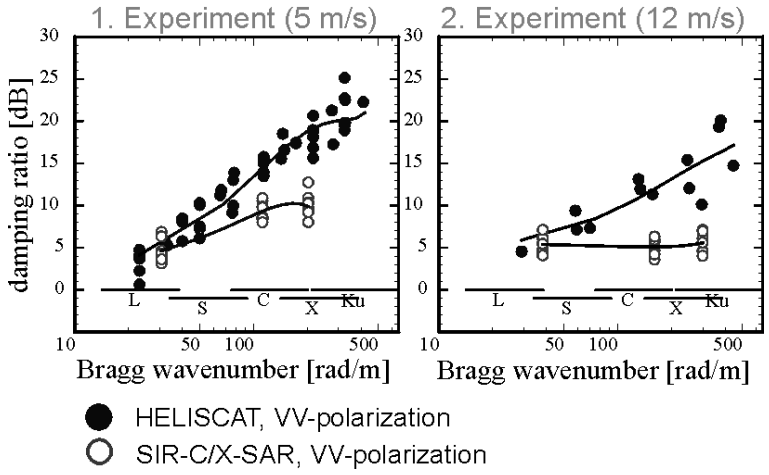

Fig. 9. Comparison of the radar contrast caused by the deployed OLA slicks during both shuttle missions in April (**left panel**) and October (**right panel**), 1994. The solid circles denote results obtained by HELISCAT, the open circles denote results obtained from SIR-C/X-SAR data. Note that in both cases, SIR-C/X-SAR measured lower damping ratios than HELISCAT

7 References

Alpers W and Hühnerfuss H (1988) Radar signatures of oil films floating on the sea and the Marangoni effect. J Geophys Res 93: 3642–3648

Donelan MA and Pierson WJ (1987) Radar scattering and equilibrium ranges in wind-generated waves with application to scatterometry. J Geophys Res 92: 4971–5029

Gade M (1996) Untersuchungen zur Abbildung biogener und anthropogener Oberflächenfilme auf dem Meer mit Hilfe von Radarsensoren. Dissertation, Univ. of Hamburg; Shaker, Aachen, 176 pp

Gade M and Redondo JM (1999) Marine pollution in European coastal waters monitored by the ERS-2 SAR: a comprehensive statistical analysis, Proceed Intern Geosci Remote Sens Sympos (IGARSS) '99, IEEE, Piscataway, NJ, USA, 1375-1377

Gade M, Alpers W, Hühnerfuss H, Masuko H and Kobayashi T (1998a) The imaging of biogenic and anthropogenic surface films by a multi-frequency multi-polarization synthetic aperture radar measured during the SIR-C/X-SAR missions. J Geophys Res 103: 18851–18866

Gade M, Alpers W, Ermakov SA, Hühnerfuss H and Lange PA (1998b) Wind-wave tank measurements of bound and freely propagating gravity-capillary waves. J Geophys Res 103: 21997–22010

Gade M, Alpers W, Hühnerfuss H, Wismann VR, and Lange PA (1998c) On the reduction of the radar backscatter by oceanic surface films: scatterometer measurements and their theoretical interpretation. Remote Sens Environ 66: 52-70

Gade M, Scholz J and v.Viebahn C (2000) On the detectability of marine oil pollution in European marginal waters by means of ERS SAR imagery. Proceed Intern Geosci Remote Sens Sympos (IGARSS) '00, IEEE, Piscataway, NJ, USA, 2510-2512

Hasselmann K (1960) Grundgleichungen der Seegangsvoraussage. Schiffstechn 7: 191-195

Hühnerfuss H (1986) The molecular structure of the system water/monomolecular surface film and its influence on water wave damping. Habilitationsschrift, Univ. Hamburg, Dept. of Chemistry, Hamburg, Germany, 245 pp

Phillips OM (1985) Spectral and statistical properties of the equilibrium range in wind-generated gravity waves. J Fluid Mech 156: 505–531

Plant WJ (1982) A relationship between wind stress and wave slope. J Geophys Res 87: 1961–1967

Valenzuela G (1978) Theories for the interaction of electromagnetic and oceanic waves - a review. Bound Layer Meteorol 13: 61–85